Structural Dynamics of Actin during Active Interaction with Myosin: Different Effects of Weakly and Strongly Bound Myosin Heads†

Ewa Prochniewicz,*,‡ Timothy F. Walseth,§ and David D. Thomas‡

Department of Biochemistry, Molecular Biology, and Biophysics and Department of Pharmacology, University of Minnesota, Minneapolis, Minnesota 55455

Received January 9, 2004; Revised Manuscript Received June 11, 2004

ABSTRACT: We have used optical spectroscopy (transient phosphorescence anisotropy, TPA, and fluorescence resonance energy transfer, FRET) to detect the effects of weakly bound myosin S1 on actin during the actomyosin ATPase cycle. The changes in actin were reported by (a) a phosphorescent probe (ErIA) attached to Cys 374 and (b) a FRET donor-acceptor pair, IAEDANS attached to Cys 374 and a nucleotide analogue (TNPADP) in the nucleotide-binding cleft. Strong interactions were detected in the absence of ATP, and weak interactions were detected in the presence of ATP or its slowly hydrolyzed analogue ATP-γ-S, under conditions where a significant fraction of weakly bound acto-S1 complex was present and the rate of nucleotide hydrolysis was low enough to enable steady-state measurements. The results show that actin in the weakly bound complex with S1 assumes a new structural state in which (a) the actin filament has microsecond rotational dynamics intermediate between that of free actin and the strongly bound complex and (b) S1-induced changes are not propagated along the actin filament, in contrast to the highly cooperative changes due to the strongly bound complex. We propose that the transition on the acto-myosin interface from weak to strong binding is accompanied by transitions in the structural dynamics of actin parallel to transitions in the dynamics of interacting myosin heads.

Strong and Weak Binding. Force is generated upon the transition of the actin-myosin complex from states of weak binding to states of strong binding during the actomyosin ATPase cycle (Figure 1). These weak and strong interactions are determined primarily by the myosin-bound nucleotide: M·ATP and M·ADP ·P binds weakly to actin, with K_d more than 1000-fold higher than that of the strong-binding M·ADP and M (no nucleotide). The understanding of structural changes in both actin and myosin during the transition from weak to strong binding is fundamental to understanding the molecular mechanism of contractility (*1*, *2*).

Structure of Strongly and Weakly Bound Actomyosin. Electron microscopy, X-ray diffraction, and spectroscopy have shown that strongly and weakly bound actin-myosin complexes have different structures, particularly regarding the conformation of myosin relative to actin. Strongly bound myosin heads form stereospecific contacts with actin, and the regions of these contacts were proposed by fitting the crystal structures of actin and myosin into electron density maps of acto-S1 complexes (*3*−*6*). In contrast, weakly bound myosin heads are dynamically disordered (*7*−*12*), and sites of contacts with actin are more speculative (*3*, *4*).

Why We Study Actin. The majority of spectroscopic studies on structural transitions during the actomyosin ATPase cycle have been focused on myosin and have led to the conclusion that the transition from weak to strong binding is associated with structural transitions in myosin (*3*, *11*, *13*). Structural transitions in actin have attracted less attention, despite the abundance of evidence that structural perturbations of actin affect its functional interactions with myosin. Chemical modifications of rabbit skeletal actin and mutagenesis of actin in yeast, *Dictyostelium*, and *Drosophila* have been shown to affect the actomyosin interaction, with some of these perturbations having different effects on actomyosin ATPase and filament sliding (*14*−*20*). These results strongly support an active role of actin in contractility and justify the present study that focuses on actin. Figure 1 illustrates the central hypothesis of this study that actin, as well as myosin, undergoes a change in structural dynamics during the weak-to-strong transition.

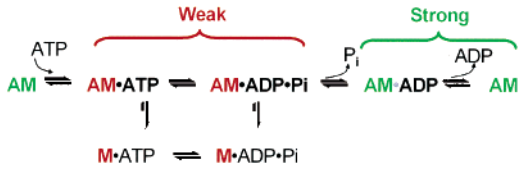

FIGURE 1: Model for the actomyosin ATPase cycle, showing the force-generating transition between weak- and strong-binding states and illustrating the central hypothesis of this study that actin, as well as myosin, undergoes a change in structural dynamics during the weak-to-strong transition.

Spectroscopy of Strongly Bound Acto-S1. Spectroscopic studies on the effect of strongly bound myosin on actin have consistently detected myosin-induced local changes, especially in the environment of actin's nucleotide-binding site and C-terminus and restriction of the microsecond time scale global dynamics of the actin filament (*21*−*28*). In our

† This work was supported by a fellowship from NIA to E.P. and by NIH grants to T.F.W. (DA11806) and D.D.T. (AR32961).

* Corresponding author. Tel: (612) 626-3344. Fax: (612) 624-0632. E-mail: ewa@ddt.biochem.umn.edu.

‡ Department of Biochemistry, Molecular Biology, and Biophysics.

§ Department of Pharmacology.

10.1021/bi049914e CCC: $27.50
Published on Web 07/30/2004

previous work with actin mutants, we concluded that strong binding of myosin is controlled by structural transitions in actin, and this raised the question whether similar transitions are involved in the mechanism of weak binding (*13*, *28*).

Spectroscopy of Weakly Bound Acto-S1. The weak-binding complex is much more difficult to study, so efforts to detect the effect of myosin on actin during weak interactions have not yet produced definitive results. The fluorescence of actin labeled at Cys 374 with pyrene iodoacetamide is quenched by strongly, but not weakly, bound myosin heads (*29*), suggesting that weakly bound heads do not affect the structure of actin. However, data obtained with other probes and techniques do not support this conclusion. Steady-state phosphorescence experiments with erythrosin-labeled actin suggested that the microsecond rotational mobility of F-actin is increased by S1 in the presence of ATP but decreased in the absence of ATP (*25*). Different effects of weakly and strongly bound heads were also detected by fluorescence microscopic observation of actin bending motions (*30*) and by polarized fluorescence of phalloidin-FITC labeled F-actin in skinned muscle fibers (*31*). On the other hand, changes in the microsecond rotational motions of spin-labeled actin induced by strongly and weakly bound S1, detected by ST-EPR, were the same (*32*). These inconsistencies are probably due to the variety of methods applied to create substantial amounts of weakly bound ternary complexes (A·M·ATP/A·M·ADP·P), and the variety of detection techniques having different sensitivities to changes in actin's structure and dynamics.

Goal of This Paper. The present work is focused on the hypothesis that there is a weak-to-strong structural transition in actin, parallel to that detected in myosin (*13*). This study employs two complementary spectroscopic methods, time-resolved phosphorescence anisotropy (TPA)[1] and fluorescence resonance energy transfer (FRET). Our previous work has demonstrated the high sensitivity of TPA to large-scale (global) structural transitions in actin (*33*), while our FRET experiments are designed to detect changes in the internal (local) structural dynamics of the actin protomer. The spectroscopic experiments performed in the presence of ATP were accompanied by biochemical assays determining actin-activated ATPase rates and K_d of the weak-binding complex, to ensure that a significant fraction of actin is occupied by weakly bound myosin heads while the acto-myosin ATPase remains in steady state during data acquisition. In an attempt to assign structural transitions in actin to a distinct ternary complex A·M·N, we have used two nucleotide transition state analogues, ATP-γ-S and ADP·V_i, which have been used previously to trap transient M·N states in the absence of actin.

The results presented in this paper show that actin weakly bound to S1 assumes a new intermediate state that is distinct from the strongly bound state in two ways: (a) the actin filament has microsecond rotational dynamics intermediate between that of free actin and the strongly bound complex and (b) S1-induced changes in actin are not propagated along the filament.

[1] Abbreviations: ErIA, erythrosin iodoacetamide; IAEDANS, 5-((((2-iodoacetyl)amino)ethyl)amino)naphthalene-1-sulfonic acid; S1, myosin subfragment 1; TPA, transient phosphorescence anisotropy; HPLC, high performance liquid chromatography; FRET, fluorescence resonance energy transfer.

MATERIALS AND METHODS

Preparation of Muscle Proteins. Skeletal muscle actin was prepared from rabbit skeletal muscle as described previously (*33*), by extracting acetone powder with cold water, polymerizing with 30 mM KCl for 1 h at room temperature, and centrifuging for 1 h at 200 000*g*. The pellet was suspended in G-Mg buffer (5 mM Tris pH 7.5, 0.5 mM ATP, 0.2 mM $MgCl_2$). Actin was pure on SDS-PAGE. Myosin subfragment 1 (S1) was obtained by α-chymotryptic digestion of myosin from rabbit skeletal muscle.

Labeling of Actin with Optical Probes. Labeling of actin at Cys 374 with ErIA (erythrosin iodoacetamide) or IAEDANS (5-((((2-iodoacetyl)amino)ethyl)amino)naphthalene-1-sulfonic acid) probes was performed as described previously (*28*). Actin (48 μM) was polymerized with 2 mM $MgCl_2$ in 20 mM Tris (pH 7.5), and the dye, freshly dissolved in DMF, was added at a concentration of 480 μM. After 2 h incubation at 25 °C, the labeling was stopped by 5 mM DTT, actin was ultracentrifuged for 1 h at 200 000*g*, pellets were suspended in G-Mg-buffer and clarified by 10 min centrifugation at 300 000*g*, and actin was polymerized for 30 min at 25 °C by adding 2 mM $MgCl_2$. After ultracentrifugation for 1 h at 200 000*g*, pellets were suspended in Mg-F buffer (3 mM $MgCl_2$, 10 mM Tris, pH 7.5) containing 0.2 mM ATP, and the labeled F-actin was immediately stabilized against depolymerization and denaturation by adding 1.5 molar equivalents of phalloidin. The extent of labeling, determined by measuring absorbance of labeled actin at 538 nm (ErIA) and 336 nm (IAEDANS), was 0.9 and 0.7 mol of dye/mol of actin, respectively.

To label IAEDANS-actin with ATPTNP, IAEDANS-labeled actin (not stabilized with phalloidin) was sonicated on ice for 2 min in 10 s bursts in Mg-F buffer containing 0.6 mM TNPATP. After ultracentrifugation (1 h at 200 000*g*), pellets were suspended in the Mg-F buffer containing 0.6 mM TNPATP instead of ATP, and the donor-acceptor labeled F-actin was immediately stabilized by adding 1.5 molar excess of phalloidin.

Actin was labeled with pyrene iodoacetamide as described previously (*34*), with slight modifications. Actin (48 μM) was polymerized with 0.1 M KCl in 1 mM NaN_3 and 20 mM Tris (pH 7.5), and the dye, freshly dissolved in DMF, was added at a concentration of 96 μM. After 18 h incubation at 23 °C, the labeling was stopped by 5 mM DTT, and actin was ultracentrifuged for 1 h at 200 000*g*. The following steps of depolymerization, polymerization, suspending final pellet of pyrene-actin in Mg-F buffer and stabilization by phalloidin were identical as described previously for ErIA-F-actin. Labeling of S1 with IASL (4-(2-iodoacetamido)-2,2,6,6-tetramethyl-1-piperidinyloxy) was performed as described previously (*35*).

Preparation of the S1·ADP·V_i Complex. Two mL of S1 (30 μM) in 50 mM Tris (pH 8), 1 mM $MgCl_2$, and 0.2 mM ADP was incubated with 0.2 mM orthovanadate (V_i) in the dark for 15 min at 25 °C, then exhaustively dialyzed (in the dark) against Mg-F buffer (*36*).

Protein Concentration. The concentration of unlabeled proteins was measured by ultraviolet absorption, assuming molar extinction coefficients of 0.63 mg mL^{-1} cm^{-1} for actin at 290 nm and 0.75 mg mL^{-1} cm^{-1} for S1 at 280 nm. The

concentration of labeled actin was measured with the Bradford protein assay (*37*) using unmodified actin as a standard. The ErIA label did not affect the readings at 595 nm: control experiments showed that the ErIA has a negligible absorption at this wavelength.

Removal of Free Nucleotide from F-Actin. F-Actin stabilized with phalloidin was treated for 2 min at 4 °C with 1:3.5 volume of Dowex 1 suspended 1:1 (vol/vol) in Mg-F buffer, the resin was removed by 2 min centrifugation in a microfuge, and actin was immediately supplemented with phalloidin (0.3 mol of phalloidin to mol of actin) to compensate for the removal of free phalloidin by Dowex 1. Dowex 1 treatment resulted in removal of more than 99% of free nucleotide, as determined by measuring the UV absorbance at 260 nm of the supernatant after centrifugation.

HPLC Analysis of ATP-γ-S. Commercial samples of ATP-γ-S were analyzed on a MonoQ HPLC column by a nonlinear gradient elution with TEAB (triethylaminobicarbonate) buffer. Integration of peaks indicated that the ADP content is typically about 10% in the commercial sample. The fractions containing purified ATP-γ-S were desalted by repeated cycles of methanol washing and drying, but during this process, the ADP levels returned to levels comparable to or higher than the original content. Therefore, further experiments were performed using commercial ATP-γ-S.

Determination of ATP-γ-S Hydrolysis Rate. S1 (2.4−12 μM) was incubated at 25 °C without or with actin (2.4−47 μM) in the presence of 1−3 mM ATP-γ-S in Mg-F buffer, and at time intervals, the reaction was terminated by precipitating proteins in 0.5 M perchloric acid. After removal of the precipitate by centrifugation, the acid was removed by shaking with a 3:1 mixture (v/v) of 1,1,2-trichloro trifluoroethane and 1-tri-*n*-octylamine, and the aqueous phase containing products of hydrolysis (ADP and Pi) was analyzed for ADP on HPLC, as described previously. The fraction of ADP at each time point was calculated as a ratio of peak area of ADP to the sum of the peak areas of ADP and unhydrolyzed ATP-γ-S remaining in the sample. The amount of liberated thiophosphate was determined in parallel experiments using radioactive ATP-γ-S and estimated by analysis of PET-cellulose TLC plates. The results were consistent with the amounts of ADP detected by HPLC.

Affinity of Weak Binding of S1 to Actin. S1, at a final concentration of 0.27 μM (in the presence of ATP) or 2.7 μM (in the presence of ATP-γ-S), was added to increasing concentrations (12−71 μM) of phalloidin-stabilized actin (unlabeled or labeled) in Mg-F buffer. Three mM ATP or 3 mM ATP-γ-S was added, and samples were immediately ultracentrifuged 15 min at 300 000*g* at 25 °C (Beckman TL 100 ultracentrifuge) to separate actin-bound and free S1. The concentration of free S1 in the presence of ATP was determined by measuring the NH_4Cl-CDTA ATPase activity of the supernatant in 0.8 M NH_4Cl, 0.12 M CDTA, 0.1 M Tris pH 7.5, 4 mM ATP (*28*), with P_i determined by the malachite green method (*38*). The concentration of free S1 in the presence of ATP-γ-S was determined by measuring the protein concentration in the supernatant (*37*): the enzymatic method was not applicable since ATP-γ-S inhibits the ATPase activity of S1. The dissociation constant for binding of S1 to actin (K_d = [A][S1]/[A·S1]) was calculated by fitting data to the ligand-binding equation using Origin 6.0.

$$[A\cdot S1]/([A\cdot S1] + [S1]) = [A]/([A] + K_d) \qquad (1)$$

where [A] = concentration of unoccupied actin monomers (assumed to be the same as the total concentration since actin is in large excess) and [S1] = concentration of unbound S1. Nucleotide saturation was assumed and was verified by variation of added nucleotide. Data were obtained in four to nine independent experiments, each of which included four to seven different actin concentrations.

Equation 1 can be used directly only if actin is in large excess over S1, as it was in our binding experiments. However, under spectroscopic conditions, when the goal was to bind S1 to a large fraction of actin protomers in the filament, there was typically an excess of S1 over actin. The fraction of actin protomers occupied by S1 was determined from the quadratic binding equation

$$A_b/A_t = \{(S_t + A_t + K_d) - [(S_t + A_t + K_d)^2 - 4A_tS_t]^{1/2}\}/2A_t \qquad (2)$$

where A_b is the concentration of actin occupied by S1, K_d is the apparent dissociation constant determined in the sedimentation assay (eq 1), and the total concentrations of S1 and actin are S_t and A_t, respectively.

Samples for Spectroscopic Experiments. For time-resolved phosphorescence anisotropy (TPA) experiments, phalloidin-stabilized ErIA-F-actin was diluted in Mg-F buffer to 1.2 μM, and strongly bound complexes were formed by adding increasing concentrations of S1 (0.1−30 μM), as indicated in the text. To prevent photobleaching of the dye, oxygen was removed from the sample by 5 min incubation with glucose oxidase (55 μg/mL), catalase (36 μg/mL), and glucose (45 μg/mL) (*39*). For fluorescence (FRET) measurements, phalloidin-stabilized IAEDANS F-actin (donor) and IAEDANS-TNPADP F-actin (donor−acceptor) were diluted in the same Mg-F buffer to 2.4 μM, and strongly bound complexes were formed by adding S1 to concentrations of 30 μM.

Phosphorescence and fluorescence measurements on acto-S1 were performed first on the strongly bound complexes, then ATP or ATP-γ-S (3 mM) was added directly to the cuvette, the sample was gently mixed, and measurements started typically 10−15 s after addition of nucleotide. For experiments in the presence of ATP-γ-S, free nucleotide was removed from actin by Dowex 1 treatment to enable calculation of the amount of ADP as a sum of ADP produced by hydrolysis of ATP-γ-S and ADP present in the commercial samples of ATP-γ-S.

Phosphorescence. Phosphorescence was measured at 25 °C as described previously (*33*), with slight modification of the TPA spectrophotometer. The actin-bound ErIA was excited with a vertically polarized 10 ns pulse from a XeCl-pumped (Compex 120, Lambda Physics) dye laser at 540 nm, using 5 mM coumarin 548 in ethanol, operating at a repetition rate of 100 Hz. Phosphorescence emission was extracted by a glass cutoff 670 nm filter (Corion), detected by a photomultiplier (R928, Hamamatsu), and digitized by transient digitizer (CompuScope 14100, GaGe) using time resolution 1 μs/channel. The time-resolved phosphorescence

anisotropy decay was calculated according to eq 3

$$r(t) = [I_{vv}(t) - GI_{vh}(t)]/[I_{vv}(t) + 2GI_{vh}(t)] \qquad (3)$$

where $I_{vv}(t)$ and $I_{vh}(t)$ are vertically and horizontally polarized components of the emission signal. These components were detected at 90° with a single detector and a Polaroid sheet polarizer that alternates between two orientations every 500 laser pulses. G is an instrumental correction factor, determined by performing the experiment with a solution of ErIA-labeled bovine serum albumin in 98% glycerol and adjusting G to give a residual anisotropy value of zero, the theoretical value for an isotropically tumbling chromophore. The time-dependent anisotropy decay was obtained by recording 2 or 3 cycles of 1000 pulses (500 in each orientation of the polarizer) at a laser repetition rate of 100 Hz; the time of one cycle was about 13 s. The data were analyzed in terms of final anisotropy r_f, calculated as an average anisotropy in the 0.4−0.5 ms (100 data points) time interval. Our previous work (*26*) showed that the final anisotropy is most sensitive to changes in actin's flexibility. The need for a brief time of data acquisition (before the end of the steady state), and the resulting noise in the signal required averaging a large number (100) of points to obtain a good signal-to-noise ratio.

The effect of S1 on final anisotropy r_f of actin was analyzed in terms of the linear lattice model (eq 4), as in our previous work (*26*), assuming that perturbation of one protomer in an actin filament affects a segment containing N monomers

$$r_f = r_{max} - (r_{max} - r_{actin})[1 - (A_b/A_t)]^N \qquad (4)$$

where r_{max} is the maximum anisotropy where all protomers are saturated with S1, r_{actin} is the anisotropy of free actin, A_b is the concentration of actin protomers with bound S1, and A_t is the total concentration of actin. The r_{max} in the strongly bound complex was calculated as an average anisotropy of actin saturated with S1 (1.2 μM actin, 1.2−36 μM S1). The r_{max} in the weakly bound complex was calculated as $[r_{obs} - r_{FA}(1 - x_b)]/x_b$, where r_{obs} is the anisotropy measured at given concentration of added S1, r_{FA} is the anisotropy of free F-actin, and x_b is the A_b/A_t (eq 2) fraction of actin protomers occupied by S1.

Fluorescence. Steady-state fluorescence was measured in the Spex Fluorolog fluorometer at 25 °C. Time-resolved fluorescence was measured with a prototype instrument from Dakota Technology, Inc. (Fargo, ND) at 25 °C. The actin-bound IAEDANS was excited with the third harmonic (355 nm) of a 1 ns pulse from Nd:YAG laser (9 kHz repetition rate). Time-dependent fluorescence emission $I(t)$ was extracted by a 440 nm glass cutoff filter, detected with the emission polarizer at the magic angle, and digitized with a digital oscilloscope (Tektronics TDS 3032B) using a dwell time of 0.5 ns/channel; signal recording was completed within 20 s.

Time-dependent fluorescence emission $I(t)$ was analyzed by fitting to a sum of three exponential terms plus a scattering component (eq 5). Increasing the number of components to three provided equal quality fits, as judged from the residuals, for donor in the absence and presence of acceptor.

$$I(t) = \text{Scat}\delta(0) + A_1\exp(-t/\tau_1) + A_2\exp(-t/\tau_2) + A_3\exp(-t/\tau_3) \qquad (5)$$

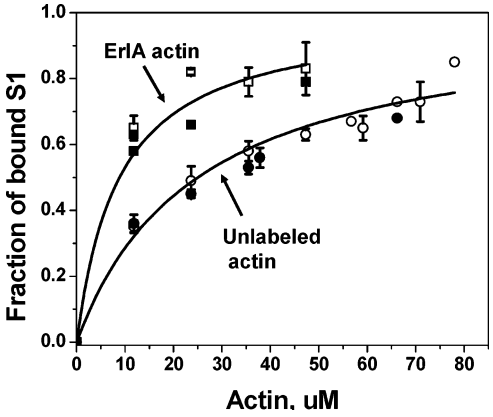

FIGURE 2: Binding of S1 to unlabeled and ErIA labeled actin in the presence of ATP (open symbols) and ATP-γ-S (closed symbols). The curves were obtained by fitting data to eq 1. Three mM $MgCl_2$, 10 mM Tris pH 7.5, 3 mM ATP, and 3 mM ATP-γ-S. S1: 0.27 μM (ATP) and 2.7 μM (ATP-γ-S).

Scat is the amplitude of scattered light, $\delta(0)$ is the delta function, A_i are amplitudes of fluorescence intensity decay, and τ_i are fluorescence lifetimes. The expression was convoluted with an excitation function $L(t)$ obtained from light scattered from a glycogen suspension, detected without the cutoff filter. This convolution was then fit to the data using an iterative nonlinear least-squares simulation using the Marquardt algorithm. The average lifetime $\langle\tau\rangle$ of donor (IAEDANS) in the absence and presence of acceptor (TNPADP) was determined as

$$\langle\tau\rangle = (\Sigma A_i\tau_i)/\Sigma A_i \qquad i = 1,2,3 \qquad (6)$$

The efficiency of energy transfer E was calculated from the average lifetime of donor in the presence (τ_{DA}) and the absence (τ_D) of acceptor

$$E = 1 - (\tau_{DA}/\tau_D) \qquad (7)$$

The distance R between the probes, corresponding to the energy transfer efficiency E, was calculated as

$$R = R_0[(1 - E)/E]^{1/6} \qquad (8)$$

where R_0 is the distance where $E = 50\%$; R_0 for the IAEDANS-TNPADP pair in actin was assumed as 40.3 Å (*40*) and corrected for the observed effect of S1 on the fluorescence lifetime.

Reagents. The phosphorescent dye ErIA and fluorescent dye IAEDANS and TNPATP were purchased from Molecular Probes (Eugene, OR) and stored at −20 °C. ATP, phalloidin, and Dowex 1 were obtained form Sigma (St. Louis, MO). ATP-γ-S was obtained from Roche Chemicals. All other chemicals were of reagent grade.

RESULTS

Binding of S1 to Actin in the Presence of ATP. The binding of myosin S1 to unlabeled and ErIA-labeled actin in the presence of ATP was measured by cosedimentation in low ionic strength buffer under the same conditions as in spectroscopic experiments (Figure 2). The affinity of S1 for unlabeled actin, expressed as the dissociation constant K_d = 25.0 ± 1.5 μM, was in the range of affinities reported previously (*41*−*43*).

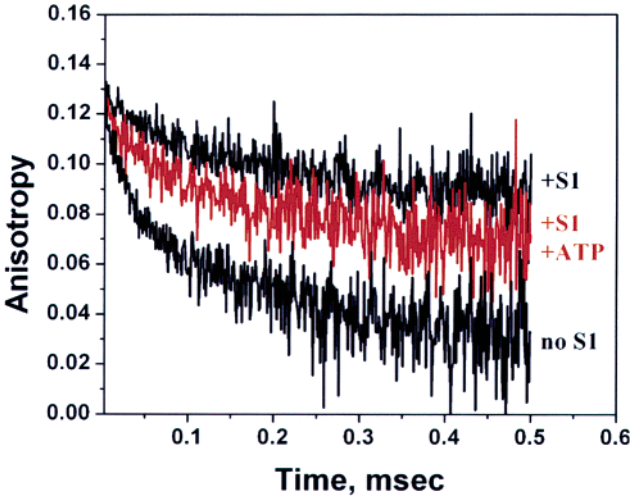

FIGURE 3: Effect of S1 (10 μM) on TPA of actin in the absence and presence of 3 mM ATP. Each decay represents 2 cycles of 1000 laser pulses.

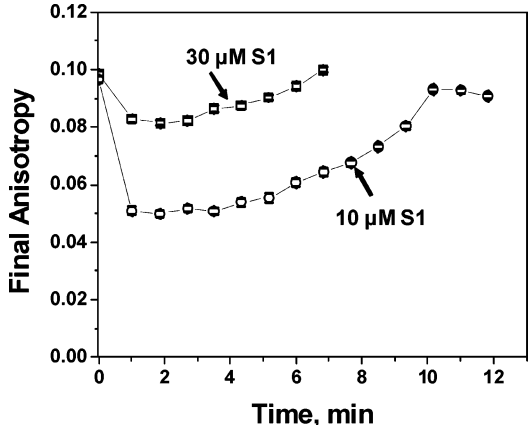

FIGURE 4: Time-course of changes in the final anisotropy of actin (1.2 μM) during interaction with S1 (10 and 30 μM) in the presence of 3 mM ATP, added at time = 0. Each anisotropy decay was acquired by recording 3 cycles of 1000 laser pulses.

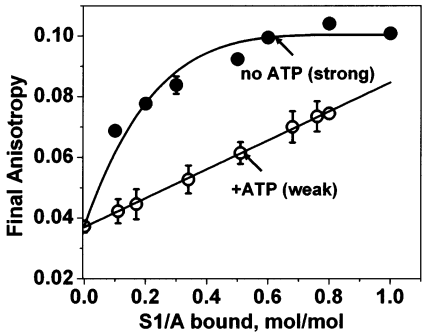

FIGURE 5: Effect of S1 on the final anisotropy r_f of actin (1.2 μM) in the absence (strong binding) and the presence (weak binding) of ATP. Each data point in the presence of ATP was calculated from the average of the first three to four decays recorded during the steady state, as illustrated in Figure 4. Curves show the best fits to the linear lattice model (eq 4).

Labeling of Cys 374 of actin with ErIA, followed by stabilization with phalloidin, did not inhibit functional interaction with myosin. The ErIA-actin bound myosin heads in the absence and presence of ATP and activated myosin ATPase. Strong binding was not affected by labeling (*28*), but ErIA labeling decreased K_d for weak S1 binding by about 3-fold, to 8.8 $\pm$ 1.5 μM (Figure 2) and V_{max} of actin-activated ATPase by about 30% (*27*). Most important, phalloidin-rhodamine ErIA-F-actin was motile in the in vitro motility assay, with a velocity similar to that of unlabeled actin (data not shown). We conclude that ErIA labeling followed by stabilization with phalloidin is suitable for detecting structural transitions involved in functional actin-myosin interactions (Figure 1). The increased affinity for myosin was beneficial since it allowed significant weak binding (high A_b/A_t in eq 2) at S1 concentrations low enough to result in hydrolysis of less than half of the available ATP during the course of TPA data acquisition.

Effect of S1 on TPA of Actin in the Presence of ATP. Figure 3 illustrates how S1 affects TPA of actin in the absence (strong binding) and in the presence (weak binding) of ATP. The anisotropy in the presence of ATP was lower than that in rigor but higher than that of free actin, suggesting that actin assumes a state intermediate between free and strongly bound states.

Detection of actin dynamics during weak interaction with S1 requires acquisition of TPA decays during the steady state of the actomyosin ATPase cycle. Therefore, in each experiment, a series of consecutive decays was recorded after addition of ATP, and data analysis was limited to decays with final anisotropy that was constant in time. For example, Figure 4 shows the final anisotropy values obtained in consecutive decays acquired after addition of ATP to acto-S1 samples containing 10 μM S1 and 30 μM S1, where the steady-state fraction of S1-bound actin (eq 2) was 0.51 and 0.76, respectively. Data analysis was limited to the anisotropies obtained for the first three (30 μM S1) or four (10 μM S1) decays, which remained constant in time. With increasing time of data acquisition, the final anisotropies gradually increased up to the level of the strongly bound complex. The time required to reach this level (i.e., the time of hydrolysis of added ATP) was consistent with the V_{max} (14 s^{-1}, ref *27*) of the ErIA actin-activated S1 ATPase. *This result shows directly that the acto-S1 complex was in the steady state of active ATP hydrolysis throughout TPA measurements.*

The effect of weakly bound S1 on the final anisotropy of actin, in comparison with the effect of strongly bound S1, is shown in Figure 5. Strong binding (no ATP) was stoichiometric due to the high affinity of S1 for actin (K_d < 0.03 μM, data not shown). The values on the horizontal axis (mol of S1 bound per mol of actin during data acquisition) were calculated from eq 2 using the K_d value determined in the cosedimentation assay (Figure 2, eq 1). Both weak- and strong-binding complexes increase the anisotropy, indicating restriction of actin's microsecond dynamics, but at all levels of bound S1, the effect of the weak complex is significantly less than that of the strong complex. Fits to the linear lattice model (eq 4) show that there are significant differences between the effects of strongly and weakly bound S1 on both extent and cooperativity of this restriction. The extent of the effect for actin weakly bound to S1, indicated by the maximum anisotropy, r_{max}(weak) = 0.084 $\pm$ 0.002, was significantly less than that for actin strongly bound to S1, r_{max}(strong) = 0.100 $\pm$ 0.002. Furthermore, while the effect of strongly bound S1 on actin's anisotropy was highly cooperative (N = 4.6), the effect of weakly bound S1 was not cooperative (N = 1), indicating that the changes are not propagated along actin filament. These differences between the effects of weakly and strongly bound S1 on actin's dynamics

suggests that actin, like myosin, undergoes a weak-to-strong structural transition during the actomyosin ATPase cycle.

These results show clearly that actin structural dynamics is affected differently by the strong- and weak-binding complexes. However, there are two proposed biochemical states that correspond to weak binding, A·S1·ATP and A·S1·ADP·P, so it is not entirely clear which of these states we have just characterized. To resolve this question, we carried out experiments designed to perturb the distribution between these two weak-binding states.

Effect of Cys707-Modified S1 on Actin's Dynamics. It has been shown that blocking SH1 (myosin Cys 707) with the iodoacetamide spin label (IASL) affects the equilibrium constant for the ATP hydrolysis step, shifting the equilibrium substantially toward the prehydrolysis state S1·ATP, at the expense of the posthydrolysis state S1·ADP·P (*44*). For unlabeled S1, in the absence of actin, approximately 70% of the myosin molecules are in the posthydrolysis state, while for spin-labeled S1, this value decreases to about 30% (*35*). Therefore, we repeated our experiments with IASL-S1. We found that the spin label caused no significant difference in either the K_d for the binding of S1 to actin, nor the effect of S1 on actin TPA, in the presence and absence of ATP (data not shown). The predominant weakly bound state in the presence of IASL-S1 is almost certainly A·M·ATP. Therefore, this result has two important implications: (a) changes induced in the structural dynamics of actin by the M·ATP and M·ADP ·P states of S1 are either not distinguishable or the M·ADP ·P state does not significantly bind to and affect actin's dynamics, as suggested by kinetic studies (*45*), and (b) the structural dynamics of actin during weak interactions can be correlated with structural states of myosin detected using Cys707-labeled S1 (*13*). This is important because numerous spectroscopic studies on structural transitions in myosin during the actomyosin ATPase cycle have been performed using myosin modified at Cys 707 with various optical and spin probes (*13*).

Interaction of Actin with S1 in the Presence of Nucleotide Analogues. Another possible approach to distinguish between the pre- and posthydrolysis states is to trap them with nucleotide analogues. Since nucleotide analogues have been used successfully to trap myosin in distinct intermediate states of the myosin ATPase cycle in the presence of nucleotide and phosphate analogues, it seems plausible that the same analogues can stabilize distinct states of the ternary A·M·N complexes (*43*, *46*, *47*). We selected two analogues, ATP-γ-S, which stabilizes an analogue of the prehydrolysis weak-binding M·ATP state (*46*, *48*, *49*), and ADP·V_i, which stabilizes an analogue of the weak-binding posthydrolysis M·ADP·P state (*50*−*52*).

The interaction of S1 with actin in the presence of ATP-γ-S was measured under the same conditions as in the presence of ATP. Control experiments showed that increasing the concentration of ATP-γ-S from 0.2 to 3 mM did not affect the amounts of weakly bound S1 (i.e., S1 was saturated with nucleotide). The affinity of S1 for actin in the presence of ATP-γ-S was essentially the same as in the presence of ATP (Figure 2) (*43*), supporting the proposal that S1·ATP-γ-S is an analogue of the S1·ATP intermediate in interaction with actin. Since ATP-γ-S is slowly hydrolyzed by S1, independently of the presence of actin (0.20 ± 0.02 (mean $\pm$ SD) mol ADP s^{-1} mol^{-1} S1 in the absence and 0.26 ± 0.10 (mean $\pm$ SD) mol ADP s^{-1} mol^{-1} S1 in the presence of actin), we performed control experiments to ensure that the TPA is acquired during the steady state, in the presence of ATP-γ-S, as well as in the presence of ATP.

Table 1: Effect of ATP and ATP-γ-S on the Final Phosphorescence Anisotropy of Actin[a]

acto-S1	5 μM S1	10 μM S1
no nucleotide	0.097 ± 0.002	0.103 ± 0.004
ATP-γ-S	0.073 ± 0.002	0.079 ± 0.002
ATP	0.056 ± 0.002	0.064 ± 0.002
no S1	0.041 ± 0.001	

[a] Mean $\pm$ SEM, $n = 3-4$.

The effect of S1 on the phosphorescence anisotropy of actin in the presence of ATP-γ-S was qualitatively similar to that of ATP, giving values intermediate between those of free actin and actin strongly bound to S1 (Table 1). This result adds support to the conclusion that the ternary A·M·N complex detected in the presence of ATP is A·M·ATP. On the other hand, the anisotropy is 20−30% higher in the presence of ATP-γ-S than in the presence of ATP, indicating that the effects of ATP-γ-S on the ternary complex are not identical to those of ATP. This higher anisotropy cannot be explained by increased S1 binding since the affinity of S1 for actin in the presence of ATP-γ-S is the same as in the presence of ATP (Figure 2, ref *43*). Another possibility, suggested previously (*43*), is that the affinity of ATP-γ-S for S1 may be weak enough, in comparison with that of ADP, so that S1·ADP produced during the hydrolysis of ATP-γ-S binds strongly to actin and increases the anisotropy. Calculations show that if this is the case, then anisotropy of actin during interaction with S1 in the presence of ATP-γ-S should be increasing, but this contradicts the experimentally observed constant level of anisotropy during the time of data acquisition. However, the assumed value for the affinity of ATP-γ-S for S1 (*43*) was only a lower limit, while the real value remains unknown (*29*, *53*), and consequently, the amounts of the S1·ADP are also unknown.

In view of uncertainties involved in calculating the amounts of strongly bound A·S1·ADP produced in the presence of ATP-γ-S, we tested the possibility of formation of this complex by measuring the effect of S1 on fluorescence of pyrene-labeled actin (*29*) under the conditions of TPA experiment (Figure 6). If S1 bound to actin in the presence of ATP-γ-S represented a mixture of strongly and weakly bound species, then at about 50% saturation of actin by S1, the fluorescence of PIA-actin in the presence of ATP-γ-S would be lower than in the presence of ATP. However, this was not observed—in the presence of both nucleotides, fluorescence was essentially the same (Figure 6), in agreement with a previous report (*54*). This shows that there is no significant accumulation of strongly bound heads in the presence of ATP-γ-S within the time range of our TPA measurements. Therefore, we conclude that the ternary complex A·M·ATP-γ-S produces effects on actin's global dynamics that are similar, but not identical, to those of ATP. The most likely explanation for the difference is the small extent of aggregation of filaments in the presence of S1 and ATP-γ-S, which is consistent with a previous report (*54*) and is supported by our observation that light scattering of acto-S1 is slightly (~12%) higher in the presence of ATP-γ-S than in the presence of ATP (data not shown).

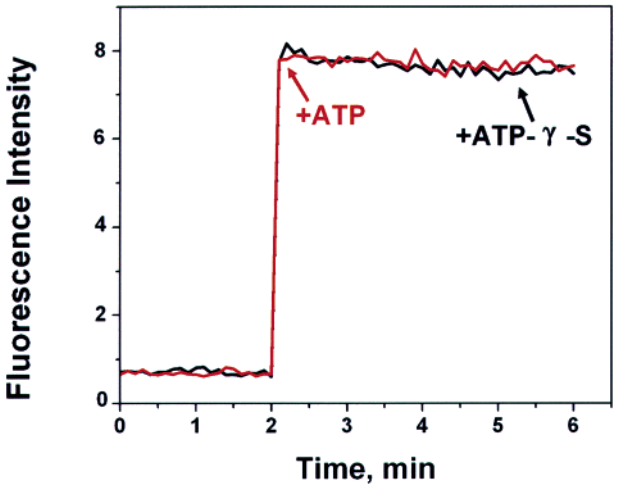

FIGURE 6: Effect of S1 (10 μM) on the fluorescence of pyrene-labeled actin in the presence of 3 mM ATP (red line) and 3 mM ATP-γ-S (black line).

Table 2: Effect of Actin on Release of V_i from S1·ADP·V_i Complex[a]

time of incubation with actin, min	ATPase rate, μM Pi/μM S1/s	
	no KCl	+50 mM KCl
0	0.12	
0.5	2.59	0.52
8	2.94	2.51
no actin, no V_i	3.08	

[a] Conditions: 3 μM S1, 28 μM actin, 3 mM $MgCl_2$, 10 mM Tris pH 7.5, 25 °C. The S1·ADP·V_i complex was added to actin, and samples were withdrawn at the indicated times for measuring NH_4Cl/CDTA ATPase. Since vanadate completely inhibits S1 ATPase, increased ATPase activity indicated release of vanadate from S1.

The addition of ADP and vanadate to myosin produces M·ADP·V_i, a stable analogue of M·ADP·P (*50*), and it has been suggested that this addition should also produce a stable analogue of the ternary complex, A·M·ADP·P (*47*). However, actin greatly decreases the stability of S1·ADP·V_i, as shown previously by the rapid recovery of S1 ATPase activity (*36*). Using this assay, we found that, under the conditions of our spectroscopic experiments, virtually all of the vanadate was released from the S1·ADP·V_i complex within 30 s after addition of actin, and a strongly bound A·S1·ADP complex was produced (Table 2), in agreement with previous fluorescence and light scattering measurements (*54*). We conclude that vanadate cannot be used to stabilize an analogue of A·M·ADP·P for a time long enough for the spectroscopic measurements of this study or a previous study (*47*).

Effect of S1 on Intramonomer FRET. The observed effect of weakly bound S1 on the actin filament's global dynamics (Figure 3) must be coupled to a change in the local structural dynamics of the actin protomer. In an attempt to detect this change, we measured the distance between Cys 374 (IAEDANS, donor) and the nucleotide binding cleft (TNPADP, acceptor), which is located in the center of the actin protomer. Labeling of Cys 374 of actin with IAEDANS, exchange of ADP into TNPADP, and stabilization of actin with phalloidin did not inhibit functional interaction with myosin: strong and weak binding affinities of S1 for actin were not affected (data not shown), and activation of S1

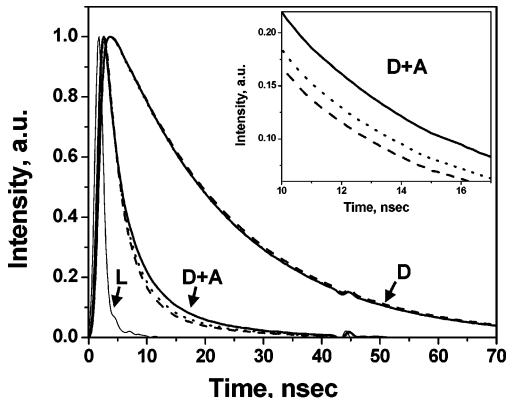

FIGURE 7: Effect of S1 (30 μM) on the time-resolved fluorescence of IAEDANS (D) and IAEDANS-TNPADP (D + A) actin (2.4 μM) in the absence and presence of 3 mM ATP-γ-S. Solid line: no S1; dotted line: +S1 +ATP-γ-S; and dashed line: +S1, no nucleotide. L is the instrument response function. The insert shows the D + A data on an expanded time base to emphasize the differences in the effects of strongly and weakly bound S1.

Table 3: Effect of S1 on the FRET Efficiency E[a]

sample	E
actin	0.802 ± 0.006 (n = 14)
actin + S1	0.828 ± 0.001 (n = 18)
actin + S1 + ATP-γ-S, total	0.816 ± 0.002 (n = 16)
actin + S1 + ATP-γ-S, bound	0.830 ± 0.008

[a] Data show mean ± SEM (n = number of experiments). Actin, 2.4 μM and S1, 30 μM.

ATPase was slightly (~13%) increased (*27*). Furthermore, the time-course of recovery of FRET efficiency from that detected immediately after addition of nucleotide to that of the strongly bound complex was consistent with the rate of hydrolysis of the added nucleotide. This indicated that, as in the TPA experiments, the fluorescent probes did not perturb the actin-myosin interaction under spectroscopic conditions and did not inhibit structural transitions involved in these interactions.

The donor fluorescence decays much more rapidly in the presence of acceptor (Figure 7). A three-exponential fit indicates that the fluorescence in the presence of acceptor has less than 10% contribution from the long-lifetime component that is predominant in the absence of acceptor, indicating that more than 90% of acceptor sites were occupied with TNPADP. It was found that precision in measuring E was maximized by calculating the average lifetime (eq 6), which decreased from 18.51 ± 0.09 ns (mean ± SEM) to 3.66 ± 0.02 ns in the absence of S1, corresponding to 80% FRET efficiency (eq 7, Table 3). This indicates that the predominant contribution to FRET comes from probes at sites separated by less than R_0 = 40.3 Å (*40*). If a single donor−acceptor distance R is assumed (eq 8), this corresponds to R = 31.9 ± 0.1 Å (mean ± SEM), which is close to the ~28 Å value predicted by the crystal structure for the distance within one protomer. We conclude that these FRET measurements reflect primarily intramonomer energy transfer.

Strong binding of S1 (in the absence of ATP) slightly but significantly increased the donor lifetime, from 18.51 ± 0.09 to 18.81 ± 0.07 ns, corresponding to a 3% increase in FRET efficiency E (Table 3) and an interprobe distance of 31.0 ±

0.1 Å, corresponding to a 0.9 ± 0.2 Å decrease in the apparent distance. This increase in E is statistically significant ($p < 0.001$) and is consistent with previous FRET studies in the strongly bound acto-S1 complex (*55*).

The effect of weakly bound S1 was measured in the presence of ATP-γ-S under conditions where the fraction of actin occupied by S1 was 0.50. As in TPA experiments, after addition of ATP-γ-S, consecutive fluorescence records were acquired to ensure that the data were acquired in the steady state, before enough hydrolysis of ATP-γ-S had occurred for recombination of actin and S1 into a strongly bound complex. (It was not possible to obtain this fluorescence data in the steady state in the presence of ATP, due to the high ATPase activity under conditions of the fluorescence experiment.) Weakly bound heads did not affect the lifetime in the absence of acceptor (18.42 ± 0.06 ns) but produced a FRET efficiency E that was significantly different from that of free actin ($p < 0.001$, Table 3). We conclude that the weakly bound actin protomer is in a structural state that is distinct from that of free actin. When the FRET efficiency of the weakly bound complex is calculated (by assuming a linear relationship), the value of E is indistinguishable from that of the strong complex (Table 3, bound). The small effects prevented a more detailed analysis in a wide range of S1 concentrations to determine cooperativity. We will continue assessment of the effects of strong and weak binding in future experiments performed with probes located in different regions of actin.

DISCUSSION

Detection of the Structural Dynamics of Weakly Bound Actin. It is a challenge to obtain data on the ternary complex containing actin, S1, and ATP because of the low affinity of actin for myosin under these conditions and because of the rapid hydrolysis of ATP by the acto-myosin complex. The experiments presented in this paper address both concerns. The quantitative determination of K_d (Figure 2) allowed us to calculate accurately the fraction of actin protomers with bound S1 (eq 2) and thus to determine the spectral properties of the ternary complex A·M·N. Determination of the rate of nucleotide hydrolysis enabled us to adjust the time of data acquisition so that all measurements were completed during the steady state of the weak interaction, before recombination of actin and S1 into a strongly bound complex.

We detected significant differences between the effects of weakly and strongly bound myosin heads on the microsecond dynamics of actin: both complexes restrict actin's rotational dynamics, but weakly bound heads have a smaller effect with much lower cooperativity than strongly bound heads (Figure 5). Indeed, the most striking difference is that strongly bound heads have a highly cooperative effect on actin, with the effect of a single bound head propagating to a group of four to five actin protomers, while a weakly bound head affects only the actin protomer to which it is bound. These TPA results are qualitatively consistent with previously reported static phosphorescence measurements showing that the dynamics of actin during interaction with S1 in the presence of ATP is different from those of free actin and strongly bound actin (*25*). Quantitative differences between these two studies are probably due to different experimental conditions and to the lack of time resolution and biochemical quantitation in the earlier study.

Our control experiments showed that our actin preparations, labeled with spectroscopic probes and stabilized by phalloidin, retain their functional interactions with myosin. Phalloidin is known to stabilize actin filaments (*56*), as evidenced by increases in persistence length (*57*), thermal stability (*58*), intersubunit contacts (*59*), and subdomain 2 stability (*60*). Nevertheless, this stabilization by phalloidin does not appear to affect the microsecond actin dynamics detected by TPA (*33*), nor does it affect actomyosin function, as measured by actin-activated myosin ATPase and in vitro motility (*14*), force generation by a single myosin head (*61*), or force generation in skinned muscle fibers (*31*). Furthermore, measurements of polarized fluorescence from phalloidin-fluorescein bound to actin in a glycerinated muscle fiber revealed structural changes in actin associated with transitions of the muscle fiber among different physiological states (*31*). Thus, it is likely that the spectroscopic observations in the present study provide reliable insight into the relationship of actin structural dynamics to function, in muscle fibers as well as in solution.

Resolution of Weakly Bound Intermediates. According to current understanding of actomyosin ATPase kinetics (*41*, *45*, *62*−*65*), weak binding involves the interaction of actin with two intermediate states of myosin, M·ATP (prehydrolysis) and M·ADP·P (posthydrolysis) (Figure 1). Which of these states have we characterized in the present study? Kinetic analysis (*45*) indicates that the affinity of M·ATP for actin is at least 20-fold higher than that of M·ADP·P, suggesting that there is a negligible population of A·M·ADP·P in the steady state. Therefore, the structural dynamics of the weak-binding ternary complex detected in the present study probably corresponds to the prehydrolysis A·M·ATP intermediate. This conclusion is further supported by the lack of an effect of the myosin Cys 707-bound spin label (see Results), which shifts the predominant ATPase intermediate from the M·ADP·P state toward the M·ATP state (*35*). The similarity of the effect of S1 on actin's anisotropy in the presence of ATP and the prehydrolysis analogue ATP-γ-S (Table 1) provides further evidence that the detected intermediate is the prehydrolysis state, A·M·ATP.

The posthydrolysis ternary complex, A·M·ADP·P, is proposed to directly precede force generation, but our attempt to stabilize actin in this state using vanadate were unsuccessful, due to the rapid release of vanadate by actin. In light of this result, and kinetic studies indicating that the affinity of M·ADP·P for actin is extremely low (*45*), it is unlikely that previous reports claiming to analyze the structure of the A·M·ADP·P complex or its analogue, stabilized by vanadate or aluminum fluoride (*47*), are valid. The structure of the posthydrolysis ternary complex remains unknown.

Comparison of Structural States of Weakly and Strongly Bound Actin. The microsecond dynamics detected by TPA of actin labeled with ErIA at Cys 374 is sensitive primarily to the global dynamics of actin, reflecting the torsional and bending motions of actin protomers relative to each other (*26*, *28*, *33*), while the fluorescence intensity (or lifetime) of pyrene or IAEDANS attached to the same site reflects primarily local (nanosecond) structural dynamics (*27*, *29*). Previous reports, confirmed in the present study (Figure 6), indicate that pyrene and IAEDANS fluorescence intensities

are affected by strongly bound, but not weakly bound, heads (*27*, *29*, *34*). In contrast, TPA shows clearly that both weakly and strongly bound heads restrict actin's global dynamics (Figure 5). Thus, we conclude that strongly bound heads affect both global and local actin dynamics, but weakly bound probes affect only global dynamics, as detected at Cys 374. This is not to say that weak binding has no structural effect on the actin protomer. Indeed, the FRET data (Figure 7, Table 3) shows that the structure of the actin protomer is significantly altered by weak myosin binding. The most likely explanation is that a weak-binding myosin head exerts its effects on the C-terminus of actin (detectable by TPA and FRET but not by pyrene fluorescence) globally, by allosteric interaction with distant sites on actin, while a strong-binding head induces an additional local structural change (detectable by pyrene-IA and TPA but not by FRET) by direct contact of myosin with the C-terminus. This conclusion is consistent with current structural models of the strongly bound actin-myosin complex. Although the C-terminus of actin was not included in the first model of the interface (*3*), it has been included in refinements of this model (*4*, *66*). The proposal that weakly and strongly bound S1 interact with different regions of actin is also consistent with studies of the N-terminus, which suggest that this region is more strongly affected by weak binding than by strong binding (*49*, *67*−*72*).

Current models of the strongly bound acto-myosin complex propose that the interface includes a large area of one actin protomer and extends into a neighboring protomer in the filament (*3*). Thus, a plausible explanation for the greater cooperativity (propagation) of effects in strong binding (Figure 5) is that the weak-binding head interacts only with one actin protomer. This is supported by (a) similar ionic strength dependence of weak binding of S1 to filamentous and monomeric actin (*73*) and (2) the inability of pyrene-actin to detect the effect of weakly bound S1 despite its high sensitivity to the changes in intermonomer interactions (*74*, *75*).

Conclusions. In summary, our results show that, in the weakly bound actin-myosin complex, (a) the actin filament has microsecond rotational dynamics (measured by TPA) intermediate between that of free actin and the strongly bound complex, (b) S1-induced changes are not propagated along the filament, in contrast to the strongly bound complex, and (c) the internal structure of weakly bound actin (measured by FRET) is distinguishable from free actin but not from strongly bound actin.

Mechanistic Implications. The differences between the effects of strongly and weakly bound S1 on actin's dynamics are probably integral to the molecular mechanism of the actomyosin ATPase cycle (Figure 8). When weakly attached to actin (in A·M·T and A·M·D·P), S1 is dynamically disordered both in its internal structure (e.g., the SH1 helix is melted (*11*, *35*, *51*)) and in the nonstereospecific attachment of the myosin catalytic domain to actin (*8*, *12*, *52*, *76*, *77*) (Figure 8, weak). Upon strong binding, myosin undergoes a disorder-to-order transition: its internal dynamics declines dramatically (*51*), the catalytic domain becomes rigidly and stereospecifically attached to actin and probably changes its mean tilt angle (*7*, *11*, *78*, *79*), and the light-chain domain also becomes more ordered and changes its mean tilt angle by 30−40°, thus changing the average shape of the head from

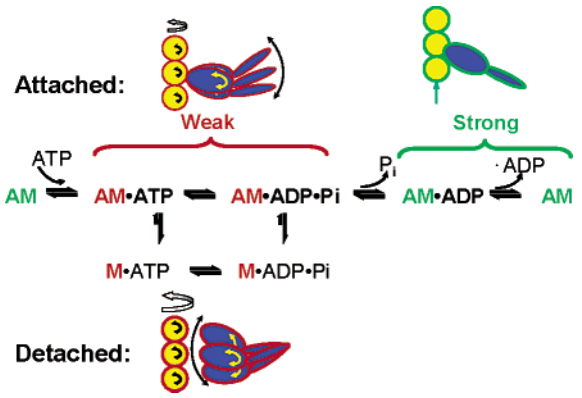

FIGURE 8: Model for the actomyosin ATPase cycle, showing the force-generating transition between weak- and strong-binding states and illustrating the principal conclusion of this study that actin, as well as myosin, undergoes a change in structural dynamics during the weak-to-strong transition.

bent to straight (*80*, *81*) (Figure 8, strong). The ordering and tilting of the light chain domain, often referred to as the lever arm rotation, is probably completed after the ordering and tilting of the catalytic domain (*79*, *81*), but these two steps are not resolved in Figure 8. As illustrated in Figure 8, the present study indicates that actin undergoes its own disorder-to-order transition as the actin-myosin complex changes from weak to strong. In the weakly bound state, actin's structural dynamics are perturbed only slightly by the dynamically attached myosin catalytic domain, while the transition to strong binding produces a more profound change, restricting the global dynamics of actin substantially and cooperatively. This weak-to-strong transition in the actomyosin complex probably involves not only the postulated closing of the actin-binding cleft of myosin (*3*, *6*, *82*−*84*) but also complementary changes at the actin side of the actomyosin interface. We hypothesize that actin's myosin-binding regions are dynamic, changing to facilitate the disordered attachment of myosin heads at the beginning of the power stroke and then to accommodate the formation of stereospecific contacts as the power stroke proceeds. Thus, we propose that the generation of force and movement by actomyosin requires that both actin and myosin undergo weak-to-strong structural transitions and that both of these transitions involve decreases in dynamic disorder.

ACKNOWLEDGMENT

We thank I. Negrashov for technical assistance with spectroscopic measurements and data analysis and O. Cornea for assistance with preparation of the manuscript.

REFERENCES

1. Kraft, T., Chalovich, J. M., Yu, L. C., and Brenner, B. (1995) Parallel inhibition of active force and relaxed fiber stiffness by caldesmon fragments at physiological ionic strength and temperature conditions: additional evidence that weak cross-bridge binding to actin is an essential intermediate for force generation, *Biophys. J. 68*, 2404−18.
2. Eisenberg, E., and Hill, T. L. (1985) Muscle contraction and free energy transduction in biological systems, *Science 227*, 999−1006.
3. Rayment, I., Holden, H. M., Whittaker, M., Yohn, C. B., Lorenz, M., Holmes, K. C., and Milligan, R. A. (1993) Structure of the actin−myosin complex and its implications for muscle contraction, *Science 261*, 58−65.
4. Mendelson, R., and Morris, E. P. (1997) The structure of the acto−myosin subfragment 1 complex: results of searches using data

from electron microscopy and X-ray crystallography, *Proc. Natl. Acad. Sci. U.S.A. 94*, 8533−8.
5. Volkmann, N., Hanein, D., Ouyang, G., Trybus, K. M., DeRosier, D. J., and Lowey, S. (2000) Evidence for cleft closure in actomyosin upon ADP release, *Nat. Struct. Biol. 7*, 1147−55.
6. Holmes, K. C., Angert, I., Kull, F. J., Jahn, W., and Schroder, R. R. (2003) Electron cryomicroscopy shows how strong binding of myosin to actin releases nucleotide, *Nature 425*, 423−7.
7. Thomas, D. D., and Cooke, R. (1980) Orientation of spin-labeled myosin heads in glycerinated muscle fibers, *Biophys. J. 32*, 891−906.
8. Svensson, E. C., and Thomas, D. D. (1986) ATP induces microsecond rotational motions of myosin heads cross-linked to actin, *Biophys. J. 50*, 999−1002.
9. Berger, C. L., Svensson, E. C., and Thomas, D. D. (1989) Photolysis of a photolabile precursor of ATP (caged ATP) induces microsecond ratational motions of myosin heads bound to actin, *Proc. Natl. Acad. Sci. U.S.A. 86*, 8753−7.
10. Frado, L. Y., and Craig, R. (1992) Structural changes induced in scallop heavy meromyosin molecules by Ca^{2+} and ATP, *J. Muscle Res. Cell Motil. 13*, 436−46.
11. Thomas, D. D., Ramachandran, S., Roopnarine, O., Hayden, D. W., and Ostap, E. M. (1995) The mechanism of force generation in myosin: a disorder-to-order transition, coupled to internal structural changes, *Biophys. J. 68*, 135S−141S.
12. Walker, M., Zhang, X. Z., Jiang, W., Trinick, J., and White, H. D. (1999) Observation of transient disorder during myosin subfragment-1 binding to actin by stopped-flow fluorescence and millisecond time resolution electron cryomicroscopy: evidence that the start of the crossbridge power stroke in muscle has variable geometry, *Proc. Natl. Acad. Sci. U.S.A. 96*, 465−70.
13. Thomas, D. D., Prochniewicz, E., and Roopnarine, O. (2002) Changes in actin and myosin structural dynamics due to their weak and strong interactions, *Results Probl. Cell Differ. 36*, 7−19.
14. Prochniewicz, E., and Yanagida, T. (1990) Inhibition of sliding movement of F-actin by cross-linking emphasizes the role of actin structure in the mechanism of motility, *J. Mol. Biol. 216*, 761−72.
15. Kim, E., Bobkova, E., Hegyi, G., Muhlrad, A., and Reisler, E. (2002) Actin cross-linking and inhibition of the actomyosin motor, *Biochemistry 41*, 86−93.
16. Johara, M., Toyoshima, Y. Y., Ishijima, A., Kojima, H., Yanagida, T., and Sutoh, K. (1993) Charge-reversion mutagenesis of *Dictyostelium* actin to map the surface recognized by myosin during ATP-driven sliding motion, *Proc. Natl. Acad. Sci. U.S.A. 90*, 2127−31.
17. Cook, R. K., Root, D., Miller, C., Reisler, E., and Rubenstein, P. A. (1993) Enhanced stimulation of myosin subfragment 1 ATPase activity by addition of negatively charged residues to the yeast actin NH2 terminus, *J. Biol. Chem. 268*, 2410−5.
18. Miller, C. J., Doyle, T. C., Bobkova, E., Botstein, D., and Reisler, E. (1996) Mutational analysis of the role of hydrophobic residues in the 338−348 helix on actin in actomyosin interactions, *Biochemistry 35*, 3670−6.
19. Miller, C. J., Wong, W. W., Bobkova, E., Rubenstein, P. A., and Reisler, E. (1996) Mutational analysis of the role of the N-terminus of actin in actomyosin interactions. Comparison with other mutant actins and implications for the cross-bridge cycle, *Biochemistry 35*, 16557−65.
20. Razzaq, A., Schmitz, S., Veigel, C., Molloy, J. E., Geeves, M. A., and Sparrow, J. C. (1999) Actin residue Glu(93) is identified as an amino acid affecting myosin binding, *J. Biol. Chem. 274*, 28321−8.
21. Yanagida, T., and Oosawa, F. (1978) Polarized fluorescence from epsilon-ADP incorporated into F-actin in a myosin-free single fiber: conformation of F-actin and changes induced in it by heavy meromyosin, *J. Mol. Biol. 126*, 507−24.
22. Thomas, D. D., Seidel, J. C., and Gergely, J. (1979) Rotational dynamics of spin-labeled F-actin in the submillisecond time range, *J. Mol. Biol. 132*, 257−73.
23. Miki, M., Wahl, P., and Auchet, J. C. (1982) Fluorescence anisotropy of labeled F-actin: influence of divalent cations on the interaction between F-actin and myosin heads, *Biochemistry 21*, 3661−5.
24. Moens, P. D., and dos Remedios, C. G. (1997) Conformational change in F-actin when myosin binds: fluorescence resonance energy transfer detects an increase in the radial coordinate of Cys-374, *Biochemistry 36*, 7353−60.
25. Ng, C. M., and Ludescher, R. D. (1994) Microsecond rotational dynamics of F-actin in ActoS1 filaments during ATP hydrolysis, *Biochemistry 33*, 9098−104.
26. Prochniewicz, E., and Thomas, D. D. (1997) Perturbations of functional interactions with myosin induce long-range allosteric and cooperative structural changes in actin, *Biochemistry 36*, 12845−53.
27. Prochniewicz, E., and Thomas, D. D. (1999) Differences in structural dynamics of muscle and yeast actin accompany differences in functional interactions with myosin, *Biochemistry 38*, 14860−7.
28. Prochniewicz, E., and Thomas, D. D. (2001) Site-specific mutations in the myosin binding sites of actin affect structural transitions that control myosin binding, *Biochemistry 40*, 13933−40.
29. Geeves, M. A., Jeffries, T. E., and Millar, N. C. (1986) ATP-induced dissociation of rabbit skeletal actomyosin subfragment 1. Characterization of an isomerization of the ternary acto−S1−ATP complex, *Biochemistry 25*, 8454−8.
30. Yanagida, T., Nakase, M., Nishiyama, K., and Oosawa, F. (1984) Direct observation of motion of single F-actin filaments in the presence of myosin, *Nature 307*, 58−60.
31. Prochniewicz-Nakayama, E., Yanagida, T., and Oosawa, F. (1983) Studies on conformation of F-actin in muscle fibers in the relaxed state, rigor, and during contraction using fluorescent phalloidin, *J. Cell. Biol. 97*, 1663−7.
32. Ostap, E. M., and Thomas, D. D. (1991) Rotational dynamics of spin-labeled F-actin during activation of myosin S1 ATPase using caged ATP, *Biophys. J. 59*, 1235−41.
33. Prochniewicz, E., Zhang, Q., Howard, E. C., and Thomas, D. D. (1996) Microsecond rotational dynamics of actin: spectroscopic detection and theoretical simulation, *J. Mol. Biol. 255*, 446−57.
34. Criddle, A. H., Geeves, M. A., and Jeffries, T. (1985) The use of actin labeled with *N*-(1-pyrenyl)iodoacetamide to study the interaction of actin with myosin subfragments and troponin/tropomyosin, *Biochem. J. 232*, 343−9.
35. Ostap, E. M., White, H. D., and Thomas, D. D. (1993) Transient detection of spin-labeled myosin subfragment 1 conformational states during ATP hydrolysis, *Biochemistry 32*, 6712−20.
36. Werber, M. M., Peyser, Y. M., and Muhlrad, A. (1992) Characterization of stable beryllium fluoride, aluminum fluoride, and vanadate containing myosin subfragment 1−nucleotide complexes, *Biochemistry 31*, 7190−7.
37. Bradford, M. M. (1976) A rapid and sensitive method for the quantitation of microgram quantities of protein utilizing the principle of protein−dye binding, *Anal. Biochem. 72*, 248−54.
38. Lanzetta, P. A., Alvarez, L. J., Reinach, P. S., and Candia, O. A. (1979) An improved assay for nanomole amounts of inorganic phosphate, *Anal. Biochem. 100*, 95−7.
39. Eads, T. M., Thomas, D. D., and Austin, R. H. (1984) Microsecond rotational motions of eosin-labeled myosin measured by time-resolved anisotropy of absorption and phosphorescence, *J. Mol. Biol. 179*, 55−81.
40. Dos Remedios, C. G., and Cooke, R. (1984) Fluorescence energy transfer between probes on actin and probes on myosin, *Biochim. Biophys. Acta 788*, 193−205.
41. Chalovich, J. M., and Eisenberg, E. (1982) Inhibition of actomyosin ATPase activity by troponin−tropomyosin without blocking the binding of myosin to actin, *J. Biol. Chem. 257*, 2432−7.
42. Trayer, H. R., and Trayer, I. P. (1988) Fluorescence resonance energy transfer within the complex formed by actin and myosin subfragment 1. Comparison between weakly and strongly attached states, *Biochemistry 27*, 5718−27.
43. Resetar, A. M., and Chalovich, J. M. (1995) Adenosine 5′-(γ-thiotriphosphate): an ATP analogue that should be used with caution in muscle contraction studies, *Biochemistry 34*, 16039−45.
44. Sleep, J. A., Trybus, K. M., Johnson, K. A., and Taylor, E. W. (1981) Kinetic studies of normal and modified heavy meromyosin and subfragment-1, *J. Muscle Res. Cell Motil. 2*, 373−99.
45. White, H. D., Belknap, B., and Webb, M. R. (1997) Kinetics of nucleoside triphosphate cleavage and phosphate release steps by associated rabbit skeletal actomyosin, measured using a novel fluorescent probe for phosphate, *Biochemistry 36*, 11828−36.
46. Berger, C. L., and Thomas, D. D. (1991) Rotational dynamics of actin-bound intermediates in the myosin ATPase cycle, *Biochemistry 30*, 11036−45.

47. Xu, J., and Root, D. D. (2000) Conformational selection during weak binding at the actin and myosin interface, *Biophys. J. 79*, 1498−510.
48. Bagshaw, C. R., Eccleston, J. F., Trentham, D. R., and Yates, D. W. (1972) Transient Kinetic Studies of the Mg^{2+}-dependent ATPase of Myosin and Its Proteolytic Subfragments, *Cold Spring Harbor Symp. Quantum Biol. 37*, 127−35.
49. Hansen, J. E., Marner, J., Pavlov, D., Rubenstein, P. A., and Reisler, E. (2000) Structural transition at actin's N-terminus in the actomyosin cross- bridge cycle, *Biochemistry 39*, 1792−9.
50. Goodno, C. C., and Taylor, E. W. (1982) Inhibition of actomyosin ATPase by vanadate, *Proc. Natl. Acad. Sci. U.S.A. 79*, 21−5.
51. Ostap, E. M., Barnett, V. A., and Thomas, D. D. (1995) Resolution of three structural states of spin-labeled myosin in contracting muscle, *Biophys. J. 69*, 177−88.
52. Roopnarine, O., and Thomas, D. D. (1996) Orientation of intermediate nucleotide states of indane dione spin-labeled myosin heads in muscle fibers, *Biophys. J. 70*, 2795−806.
53. Bagshaw, C. R., Eccleston, J. F., Eckstein, F., Goody, R. S., Gutfreund, H., and Trentham, D. R. (1974) The magnesium ion-dependent adenosine triphosphatase of myosin. Two-step processes of adenosine triphosphate association and adenosine diphosphate dissociation, *Biochem. J. 141*, 351−64.
54. Geeves, M. A., and Jeffries, T. E. (1988) The effect of nucleotide upon a specific isomerization of actomyosin subfragment 1, *Biochem. J. 256*, 41−6.
55. Miki, M., and Wahl, P. (1984) Fluorescence energy transfers in labeled G- and F-actin, *Biochim. Biophys. Acta 786*, 188−96.
56. Estes, J. E., Selden, L. A., and Gershman, L. C. (1981) Mechanism of action of phalloidin on the polymerization of muscle actin, *Biochemistry 20*, 708−12.
57. Isambert, H., Venier, P., Maggs, A. C., Fattoum, A., Kassab, R., Pantaloni, D., and Carlier, M. F. (1995) Flexibility of actin filaments derived from thermal fluctuations. Effect of bound nucleotide, phalloidin, and muscle regulatory proteins, *J. Biol. Chem. 270*, 11437−44.
58. Le Bihan, T., and Gicquaud, C. (1991) Stabilization of actin by phalloidin: a differential scanning calorimetric study, *Biochem. Biophys. Res. Commun. 181*, 542−7.
59. Lorenz, M., Popp, D., and Holmes, K. C. (1993) Refinement of the F-actin model against X-ray fiber diffraction data by the use of a directed mutation algorithm, *J. Mol. Biol. 234*, 826−36.
60. Orlova, A., and Egelman, E. H. (1993) A conformational change in the actin subunit can change the flexibility of the actin filament, *J. Mol. Biol. 232*, 334−41.
61. Finer, J. T., Simmons, R. M., and Spudich, J. A. (1994) Single myosin molecule mechanics: picoNewton forces and nanometre steps, *Nature 368*, 113−9.
62. Lymn, R. W., and Taylor, E. W. (1971) Mechanism of adenosine triphosphate hydrolysis by actomyosin, *Biochemistry 10*, 4617−24.
63. Rosenfeld, S. S., and Taylor, E. W. (1984) The ATPase mechanism of skeletal and smooth muscle acto-subfragment 1, *J. Biol. Chem. 259*, 11908−19.
64. Ma, Y. Z., and Taylor, E. W. (1994) Kinetic mechanism of myofibril ATPase, *Biophys. J. 66*, 1542−53.
65. Iwamoto, H., Oiwa, K., Suzuki, T., and Fujisawa, T. (2001) X-ray diffraction evidence for the lack of stereospecific protein interactions in highly activated actomyosin complex, *J. Mol. Biol. 305*, 863−74.
66. Root, D. D., Stewart, S., and Xu, J. (2002) Dynamic docking of myosin and actin observed with resonance energy transfer, *Biochemistry 41*, 1786−94.
67. DasGupta, G., and Reisler, E. (1991) Nucleotide-induced changes in the interaction of myosin subfragment 1 with actin: detection by antibodies against the N-terminal segment of actin, *Biochemistry 30*, 9961−6.
68. DasGupta, G., and Reisler, E. (1992) Actomyosin interactions in the presence of ATP and the N-terminal segment of actin, *Biochemistry 31*, 1836−41.
69. Mornet, D., Bertrand, R., Pantel, P., Audemard, E., and Kassab, R. (1981) Structure of the actin−myosin interface, *Nature 292*, 301−6.
70. Bonafe, N., and Chaussepied, P. (1995) A single myosin head can be cross-linked to the N-termini of two adjacent actin monomers, *Biophys. J. 68*, 35S−43S.
71. Van Dijk, J., Fernandez, C., and Chaussepied, P. (1998) Effect of ATP analogues on the actin−myosin interface, *Biochemistry 37*, 8385−94.
72. Gu, J., Xu, S., and Yu, L. C. (2002) A model of cross-bridge attachment to actin in the A*M*ATP state based on X-ray diffraction from permeabilized rabbit psoas muscle, *Biophys. J. 82*, 2123−33.
73. Lheureux, K., Forne, T., and Chaussepied, P. (1993) Interaction and polymerization of the G-actin−myosin head complex: effect of DNase I, *Biochemistry 32*, 10005−14.
74. Tellam, R., and Frieden, C. (1982) Cytochalasin D and platelet gelsolin accelerate actin polymer formation. A model for regulation of the extent of actin polymer formation in vivo, *Biochemistry 21*, 3207−14.
75. Kouyama, T., and Mihashi, K. (1980) Pulse-fluorometry study on actin and heavy meromyosin using F-actin labeled with *N*-(1-pyrene)maleimide, *Eur. J. Biochem. 105*, 279−87.
76. Fajer, P. G., Fajer, E. A., and Thomas, D. D. (1990) Myosin heads have a broad orientational distribution during isometric muscle contraction: time-resolved EPR studies using caged ATP, *Proc. Natl. Acad. Sci. U.S.A. 87*, 5538−42.
77. Berger, C. L., and Thomas, D. D. (1993) Rotational dynamics of actin-bound myosin heads in active myofibrils, *Biochemistry 32*, 3812−21.
78. Cooke, R., Crowder, M. S., and Thomas, D. D. (1982) Orientation of spin labels attached to cross-bridges in contracting muscle fibres, *Nature 300*, 776−8.
79. Taylor, K. A., Schmitz, H., Reedy, M. C., Goldman, Y. E., Franzini-Armstrong, C., Sasaki, H., Tregear, R. T., Poole, K., Lucaveche, C., Edwards, R. J., Chen, L. F., Winkler, H., and Reedy, M. K. (1999) Tomographic 3-D Reconstruction of Quick-Frozen, Ca^{2+}-Activated Contracting Insect Flight Muscle, *Cell 99*, 421−31.
80. Baker, J. E., Brust-Mascher, I., Ramachandran, S., LaConte, L. E., and Thomas, D. D. (1998) A large and distinct rotation of the myosin light chain domain occurs upon muscle contraction, *Proc. Natl. Acad. Sci. U.S.A. 95*, 2944−9.
81. LaConte, L. E., Baker, J. E., and Thomas, D. D. (2003) Transient kinetics and mechanics of myosin's force-generating rotation in muscle: resolution of millisecond rotational transitions in the spin-labeled myosin light-chain domain, *Biochemistry 42*, 9797−803.
82. Volkmann, N., Ouyang, G., Trybus, K. M., DeRosier, D. J., Lowey, S., and Hanein, D. (2003) Myosin isoforms show unique conformations in the actin-bound state, *Proc. Natl. Acad. Sci. U.S.A. 100*, 3227−32.
83. Reubold, T. F., Eschenburg, S., Becker, A., Kull, F. J., and Manstein, D. J. (2003) A structural model for actin-induced nucleotide release in myosin, *Nat. Struct. Biol. 10*, 826−30.
84. Coureux, P. D., Wells, A. L., Menetrey, J., Yengo, C. M., Morris, C. A., Sweeney, H. L., and Houdusse, A. (2003) A structural state of the myosin V motor without bound nucleotide, *Nature 425*, 419−23.

BI049914E